Magneto-optical study of flux penetration and critical current densities in [001] tilt $YBa_2Cu_3O_{7-\delta}$ thin-film bicrystals

A. A. Polyanskii,* A. Gurevich, A. E. Pashitski, N. F. Heinig, R. D. Redwing, J. E. Nordman,† and D. C. Larbalestier‡
Applied Superconductivity Center, University of Wisconsin, Madison, Wisconsin 53706
(Received 23 October 1995)

Magneto-optical (MO) imaging has been used to visualize and calculate magnetic flux and current distributions at temperatures T ranging from 7 to 80 K in thin-film [001] tilt $YBa_2Cu_3O_{7-\delta}$ bicrystals with misorientation angles $3° \leqslant \theta \leqslant 10°$. A characteristic cusp in the flux distribution $B_z(x,y)$ was observed for $5° \leqslant \theta \leqslant 7°$, which is shown to indicate that the critical current density J_b across the boundary is smaller than the intragrain J_c. We use the Bean model for thin-film superconductors to calculate the observed features of the $B_z(x,y)$ distribution and to separate both the intragrain J_c and intergrain $J_b(\theta)$ independently from the MO data. The study of angular and temperature dependencies of $J_b(T,\theta)$ in bicrystals with different θ shows that $J_b(\theta)$ strongly decreases with θ above $\theta \approx 5°$. The decrease of $J_b(T,\theta)$ with temperature becomes weaker as the misorientation angle θ is increased, so the substantial difference in J_b for 5° and 7° boundaries at low T turns out to be less pronounced at liquid-nitrogen temperatures. In addition, the ratio $J_b(\theta,T)/J_c(T)$ for low-angle grain boundaries is shown to exhibit an anomalous increase with T, thus indicating that the grain boundaries can provide additional flux pinning. This is plausibly associated with the grain boundary dislocations that accommodate the misorientation of the grains.

I. INTRODUCTION

Planar crystalline defects, such as grain and twin boundaries, intergrowths and stacking faults can impose limitations on the critical current density J_c of high-T_c superconductors (HTS) because the short coherence length of these materials tends to make planar defects weakly coupled.[1] High angle grain boundaries are particularly effective barriers to current flow. There is an extensive literature on the dependence of the intergrain critical current density J_b on the misorientation angle θ of bicrystals. For example, the transport data for tilt and twist grain boundaries in $YBa_2Cu_3O_{7-\delta}$ thin-film bicrystals[2–9] indicate a strong dependence of $J_b(\theta)$. Similar behavior was also observed on Bi and Tl-based HTS thin films.[10–16] The temperature and field dependencies of J_b can vary significantly from sample to sample. For large angles θ, J_b can generally be described by modeling the grain boundaries as superconductor-insulator-superconductor or superconductor–normal-metal–superconductor long Josephson contacts, although some high angle grain boundaries do not exhibit weak link behavior.[17–21]

Studies of magnetization currents around grain boundaries[22–29] and twin boundaries[30–37] in HTS thin films, ceramics, and single crystals have been performed with the magneto-optical (MO) technique and with scanning electron microscopy.[38] The MO technique, by allowing a direct visualization of magnetic flux penetration into the sample, has shown that preferential flux penetration occurs along grain and twin boundaries, thus indicating that J_b is lower than the intragrain J_c. The qualitative dependence of the flux penetration on θ has been determined in bulk $YBa_2Cu_3O_{7-\delta}$ bicrystal,[26] but there has been no quantitative MO study of the angular dependence of the intergrain and intragrain critical current density in either bulk or thin-film samples. Such studies are of particular value, since the MO technique permits a direct observation of the evolution of **H(r)** and **J(r)** distributions for different θ, and thus permits the extraction of the $J_b(\theta,T)$ dependencies. MO studies can also be very helpful in tracing the crossover from strongly to weakly coupled grain boundaries upon increasing θ and in determining whether boundaries are uniform in their properties.[29] These characteristics may prove to be important for further optimization of polycrystalline HTS materials, especially in light of recent reports of extremely high J_c values observed in $YBa_2Cu_3O_{7-\delta}$ thick-film composites.[39–42]

In this paper we present the results of such a quantitative magneto-optical study of the flux distribution and critical current density of [001] tilt grain boundaries in thin-film $YBa_2Cu_3O_{7-\delta}$ bicrystals. The paper is organized as follows.

In Sec. II we describe the samples used in this work and present the angular dependencies of J_b obtained by transport measurements.

In Sec. III we present detailed MO images of the magnetic flux penetration into grain boundaries with θ ranging from 3° to 10°. We describe a characteristic cusp in the $B_z(x,y)$ distribution at the film center which indicates a substantial J_b across the boundary. The cusp was found to be most pronounced for $\theta \approx 5°$, decreasing both for smaller and larger θ.

In Sec. IV we interpret the observed distribution $B_z(x,y)$ within the framework of the Bean model for thin flat superconductors in a perpendicular magnetic field, H_a. For fields larger than the full penetration field, an analytical formula for $B_z(x,y)$ is obtained which qualitatively describes the observed features of $B_z(x,y)$ and the flux profiles around the boundary.

In Sec. V we propose a method to extract both J_c and J_b from the MO data and thus to study the temperature and angular dependencies of J_b without any contributions from the intragrain regions which are necessarily present in transport measurements on bicrystals. For lower angle boundaries

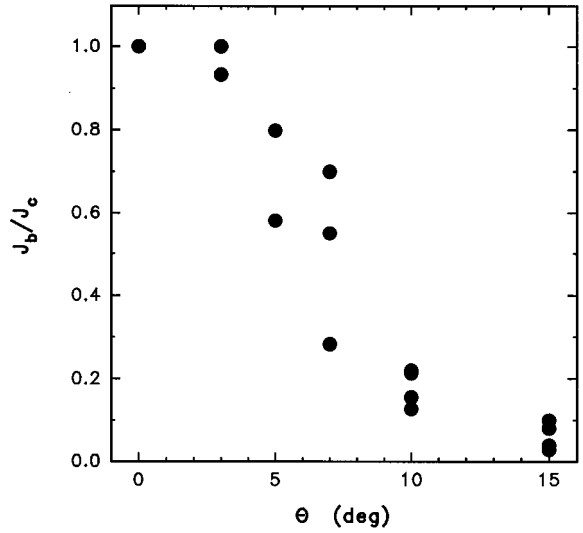

FIG. 1. Ratio of intergrain to intragrain critical current density, J_b/J_c, versus [001] misorientation angle, θ, at $T=77$ K and $H_a=0$.

($\theta \leqslant 7°$), we found that the ratio $J_b(\theta,T)/J_c(T)$ exhibits a substantial increase with T, becoming of order unity about the irreversibility line. By contrast, for the 10° bicrystal the ratio $J_b(\theta,T)/J_c(T)$ remains much smaller than 1 at all T.

II. SAMPLE GROWTH AND CHARACTERIZATION

The samples were formed by growing $YBa_2Cu_3O_{7-\delta}$, c-axis oriented films on the [001] surface of 2×10 mm symmetric tilt $SrTiO_3$ bicrystals, whose [001] axes were parallel with an accuracy better than 1°. The films were grown by pulsed deposition using a KrF pulsed laser system operated at 5 Hz and wavelength 248 nm at an energy density 1.4 J/cm^2 and 0.05 nm/pulse growth rate. The bicrystal substrates were held at approximately 760 °C in 210 mTorr oxygen during growth and then slowly cooled to room temperature in 800 mTorr oxygen. The film thicknesses ranged from 150 to 250 nm and had superconducting transition temperatures, T_c, between 88–90 K, resistance ratios $R(300\ \mathrm{K})/R(100\ \mathrm{K})$ of about 2.5, and intragrain critical current densities, J_c, in the range of 1–5 MA/cm^2 for 77 K and $H_a=0$.

We performed four probe measurements of both the intergrain and intragrain voltage-current (V-I) characteristics of our bicrystals.[40] Gold for the contacts was evaporated onto the films using a shadow mask to protect the grain boundary region, and the current and voltage taps were then photolithographically patterned onto the sample. The distance between the voltage probes was 100 μm across the grain boundary and 500 μm across the grain. The width of different bridges on the films varied between 5 and 100 μm. Different bridges were selected, depending on the capability of the power supply and the critical current I_c of the bridge. After patterning, excess $YBa_2Cu_3O_{7-\delta}$ was removed using Ar etching.

Figure 1 shows the zero field angular dependence of the ratio of intergrain to intragrain critical current density, $J_b(\theta)/J_c(\theta)$. J_b lies in the range $1–5\times10^6$ A/cm^2 for θ up to 7° but falls to $3–4\times10^5$ A/cm^2 for the 10° bicrystals. A fuller description of these results is presented by Heinig *et al.*[40] A finite grain boundary resistance appears at about 5°–7°, indicating the appearance of a significant barrier to current flow in the boundary. Transmission electron microscopy of the 10° bicrystal showed that the grain boundary contained primary grain boundary dislocations separated by comparatively undisturbed lattice. These good channels appear to close between 10° and 15°. Although there are differences of details between these films and those studied by others, their overall behavior is qualitatively similar to that observed previously.[2–5,7–16]

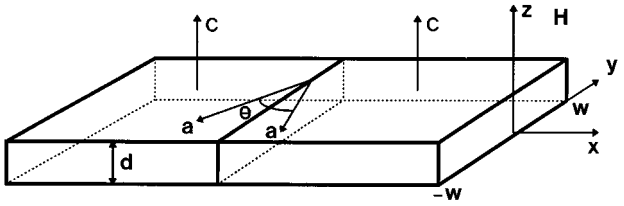

FIG. 2. Geometry of the sample and the mutual orientation of the grain boundary and external magnetic field, $H_a \| z$. For calculations the film thickness d was assumed to be negligible ($d \ll w$), and $x=y=0$ was the center of the grain boundary. θ is the tilt misorientation angle between the grains.

III. MAGNETO-OPTICAL IMAGES OF GRAIN BOUNDARIES

We used the MO technique described in Refs. 31,43,44 to image the normal field component $B_z(x,y)$ produced by the magnetization currents with a 2 μm thick Bi-doped Y-garnet indicator film placed directly onto the sample surface. MO images were taken for the magnetic field H_a applied perpendicular to the surface of the bicrystal and parallel to the crystal c axis and to the z axis of the coordinate system, as shown in Fig. 2. The grain boundary plane thus lies in the yz coordinate plane. Images were recorded on a videotape and then imported into a digital image processor in order to derive absolute values of $B_z(x,y)$ as described in Refs. 45,46.

Figures 3–6 show examples of different stages of magnetic flux penetration in the bicrystals with $\theta=3°$, 5°, and 10°. The bright regions of partial flux penetration correspond to higher values of the normal field component $B_z(x,y)$, while the dark central stripes are vortex-free regions, where only Meissner currents flow. As seen from Fig. 3, the 3° grain boundary only weakly disturbs the magnetic flux distribution, in agreement with the transport data in Fig. 1 which indicate that J_b for $\theta=3°$ is close to the intragrain J_c. By contrast, the 10° bicrystal shown in Fig. 4 exhibits two separate ''pillowlike'' flux patterns characteristic of edges of thin flat superconductors in a perpendicular field.[43,47–51] In this case the grain boundary gives rise to a strong electromagnetic decoupling of the two grains of the bicrystal, in each of which the magnetization currents become practically independent. This is again in qualitative agreement with the transport data in Fig. 1 which shows that $J_b(10°)$ is of order $0.1J_c$. The 5° and 7° bicrystals correspond to an intermediate regime between the above extremes, for which their larger values of J_b significantly affect the distribution of $B_z(x,y)$. The interesting qualitative feature of the 5° bicrystal patterns shown in Fig. 5 is a characteristic cusp in $B_z(x,y)$ which

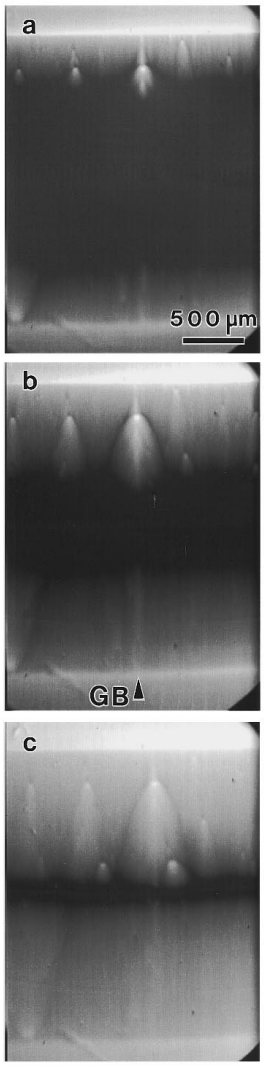

FIG. 3. MO images of different stages of magnetic flux penetration into the 3° grain boundary for ZFC at $T=7$ K and $H_a=212$ Oe, (a), 376 Oe (b), and 748 Oe (c).

bisects the center of the boundary. This cusp is a direct consequence of a significant J_b, as will be shown below. For the 7° bicrystal, the cusp in $B_z(x,y)$ was less pronounced. It should be emphasized that this cusp is not due to Meissner screening currents flowing in the central part of the film in the zero-field-cooled (ZFC) regime of incomplete flux penetration. This follows from Fig. 6 which shows the same cusp in $B_z(x,y)$ for the trapped flux in the field cooled regime for which there are no Meissner currents flowing in the film center.

Figures 7 and 8 show typical flux profiles taken in different directions with respect to the grain boundary of the 5° bicrystal. Here there is a local enhancement of $B_z(x,y)$ in the grain boundary plane, whose relative magnitude depends on the position y along the boundary. Such a flux focusing effect indicates preferential field penetration into the boundary, which is similar to the large demagnetization enhancement of $B_z(x,y)$ at the edge of a flat thin superconductor in a perpendicular field.[43,49,52–60] The flux profiles taken along the boundary $B_z(x,y)$ shown in Fig. 8 exhibit a quite different nonmonotonic behavior, which will be discussed in more detail in the next section.

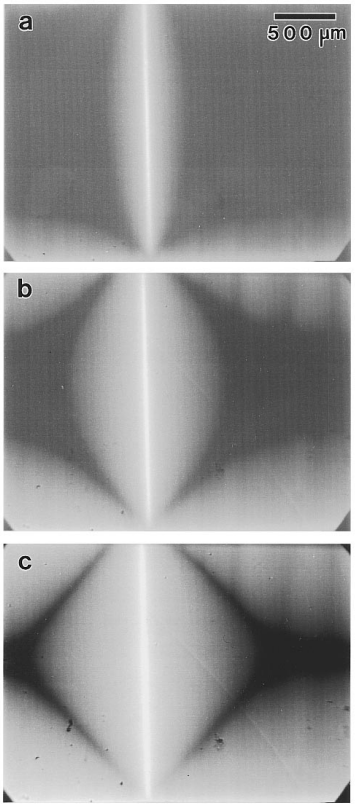

FIG. 4. MO images of different stages of magnetic flux penetration into the 10° grain boundary for ZFC at $T=7$ K and $H_a=240$ Oe (a), 480 Oe, (b), and 800 Oe (c).

Shown in Fig. 9 are representative MO images of the 5° bicrystal taken at different temperatures, the images exhibiting the characteristic field distribution $B_z(x,y)$ expected from the Bean model.[61,62] The bright regions correspond to the above-mentioned field enhancement at the grain boundary and the film edges. Darker strips which make the angle α with the film edge correspond to the regions where magnetization currents sharply change direction. For an isotropic J_c, the angle α should equal 45°,[49–51,61,62] while derivations from 45° indicate either an anisotropy of the bulk J_c,[63] or a nonzero J_b across the boundary.[36] For the samples used in this study we checked the anisotropy of J_c in the ab plane and found it to be negligible, since the MO images of the rectangular sample edge all showed α to be temperature independent and close to 45°. This is consistent with the fact that a characteristic spacing between twin planes in thin films is typically of the order of 1 μm, thus making J_c isotropic on the scale resolved by MO imaging. By contrast, as seen from Fig. 9, the angle α for the 5° bicrystal was quite different from 45° and noticeably changed with T. This fact indicates different temperature dependencies of J_c and J_b and enables us to extract both the ratio $J_b(T)/J_c(T)$ and $J_b(T)$ from the MO images, as will be shown below.

IV. BEAN MODEL CALCULATIONS

The qualitative features of the $B_z(x,y)$ distributions described above can all be accounted for by the Bean model in which the current flows around and across the grain bound-

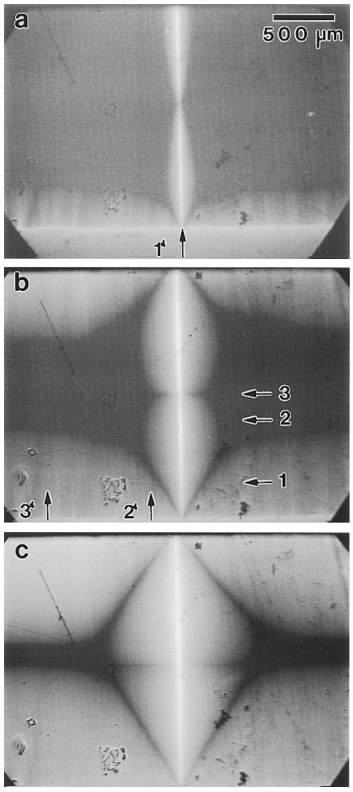

FIG. 5. MO images of different stages of magnetic flux penetration into the 5° grain boundary for ZFC at $T=7$ K and $H_a=200$ Oe (a), 400 Oe (b), and 720 Oe (c). Arrows indicate the directions along which the 1, 2, 3, $1'$, $2'$, and $3'$ profiles were taken.

ary, as is sketched in Fig. 10. Here we assume that H_a is well above the field of full flux penetration, and that J_c and J_b are both homogeneous and field independent. We also do not take account of flux creep effects, which can be neglected in the low temperature region, well below the irreversibility temperature, $T_{\rm irr}$. For the current pattern shown in Fig. 9, the critical state occupies the entire sample, so that modulus of **J** equals J_c everywhere in the bulk, and the normal component J_n crossing the grain boundary equals J_B ($J_b<J_c$). From these conditions one can easily calculate the angle α between the sample edge and the line on which the magnetization currents sharply change the direction [the so-called ''current discontinuity (d) lines'' in the terminology of Ref. 50]. From the continuity of the normal component of **J(r)** at the d lines[36] it follows that

$$\cos 2\alpha = -\frac{J_b}{J_c}. \tag{1}$$

For $J_b=0$, Eq. (1) gives the well-known result $\alpha=45°$ of the isotropic Bean model for a rectangular sample edge[49–51,61,62] (a generalization to the case of anisotropic J_c was given in Ref. 63).

Now we use the Biot-Savart law

$$B(x,y)=\mu_0\int_{-w}^{w}dy'\int_{-\infty}^{\infty}dx'\frac{(y-y')J_x(r')-(x-x')J_y(r)}{[(x-x')^2+(y-y')^2+z^2]^{3/2}} \tag{2}$$

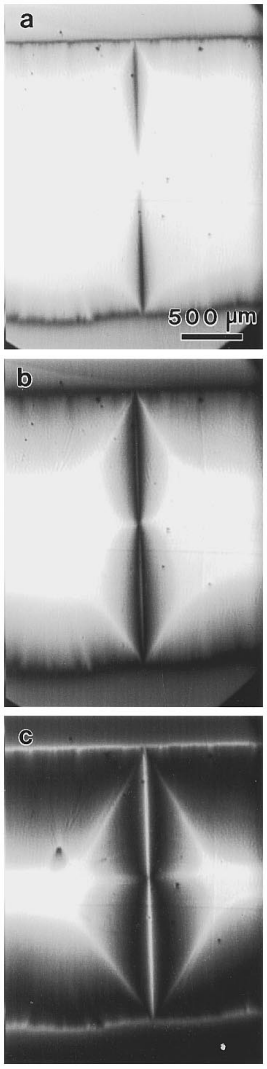

FIG. 6. MO images taken after field cooling the 5° bicrystal to $T=19$ K in $H_a=400$ Oe. $H_a=228$ Oe (a), 172 Oe (b), and 0 Oe (c).

to calculate $B_z(x,y)$ at a distance z above the surface of a thin-film superconducting strip located at $z=0$. We assume that the strip has a width $2w$ along the y axis and is infinite in the x direction perpendicular to the grain boundary. Here the thickness of the strip $d\ll w$ is assumed to be negligible, so $B_z(x,y)$ is determined by the sheet current density, $\mathbf{J(r)}=d\mathbf{j(r)}$. To describe this case, we have to take account of the distinctive features of the critical state in thin superconductors in a perpendicular field[49–59] which are rather different from the Bean model for a slab in parallel field.[61,62] For instance, there is a vortex-free region of width $2b(B_a)$ in the central part of the strip where only Meissner screening currents flow. Here

$$b(B_a)=\frac{w}{\cosh(B_a/B_0)} \tag{3}$$

and $B_0=\mu_0 J_c d/\pi$ is the characteristic field of full flux penetration.[56,57] In the MO images shown in Figs. 3–5, such vortex-free regions can be clearly seen as dark domains in the central part of the film. This Meissner region and its related geometrical barriers[58] considerably complicate calcu-

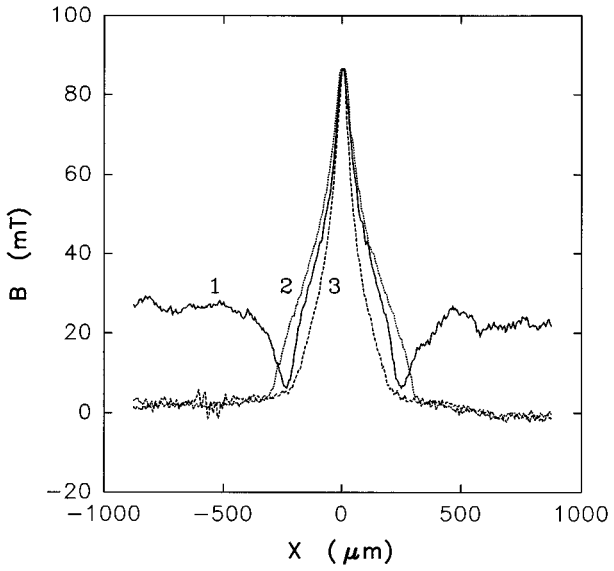

FIG. 7. Magnetic flux profiles $B_z(x,y)$ for the 5° boundary taken along the directions 1, 2, and 3 perpendicular to the grain boundary plane in Fig. 5.

lations of $B_z(x,y)$ in flat superconductors at low fields, so for simplicity we restrict ourselves to the higher field regime $B_a > B_0 \ln(2w/\lambda)$ for which the Meissner region becomes smaller than the London penetration depth λ. In this case the current distribution in a thin-film bicrystal reduces to the idealized one shown in Fig. 10, where

$$J_x = [J_c + (J_b - J_c)\,\theta(|y| - |x|\tan\alpha)]\,\mathrm{sgn}(y), \tag{4}$$

$$J_y = -\sqrt{J_c^2 - J_b^2}\,\theta(|y| - |x|\tan\alpha)\,\mathrm{sgn}(x) \tag{5}$$

and $\theta(x)$ is the step function: $\theta(x)=1$ for $x>0$ and $\theta(x)=0$ for $x<0$. After substituting Eqs. (4) and (5) into Eq. (2) and

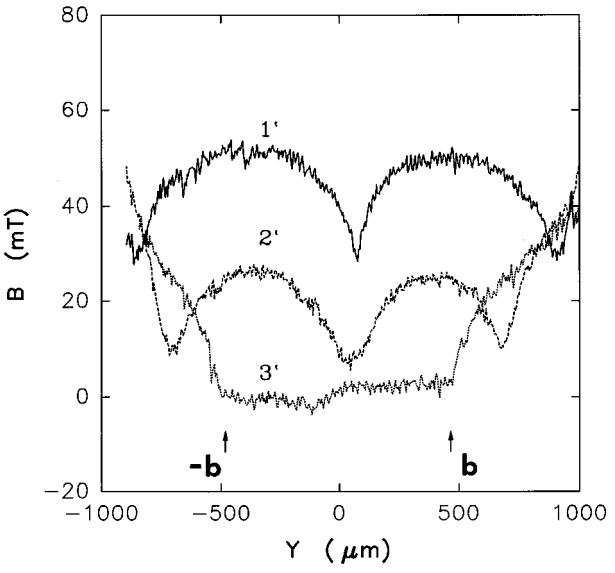

FIG. 8. Magnetic flux profiles $B_z(x,y)$ for the 5° boundary taken along the directions, $1'$, $2'$, and $3'$ parallel to the grain boundary plane in Fig. 5. $2b$ is the width of Meissner region.

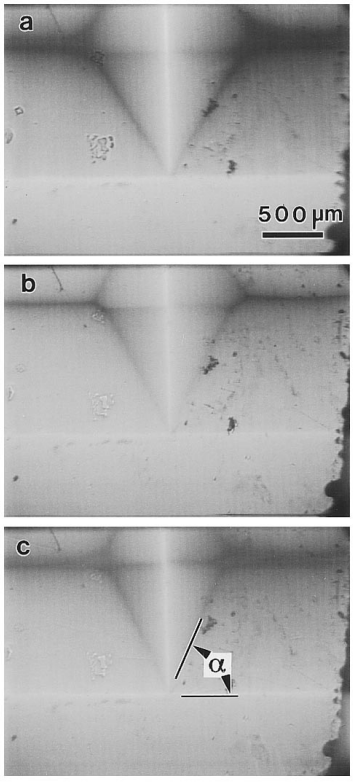

FIG. 9. MO images of flux distribution around the 5° boundary for $T=7$ K and $H_a=800$ Oe (a); $T=30$ K and $H_a=800$ Oe (b) $T=50$ K and $H_a=400$ Oe (c). α is the angle between the film edge and current discontinuity line.

integrating over x' and y', we obtain the cumbersome formulas for $B_z(x,y)$ given in the Appendix. Using this analytical expression for $B_z(x,y)$, we consider the characteristic features of $B_z(x,y)$ caused by the grain boundary and trace

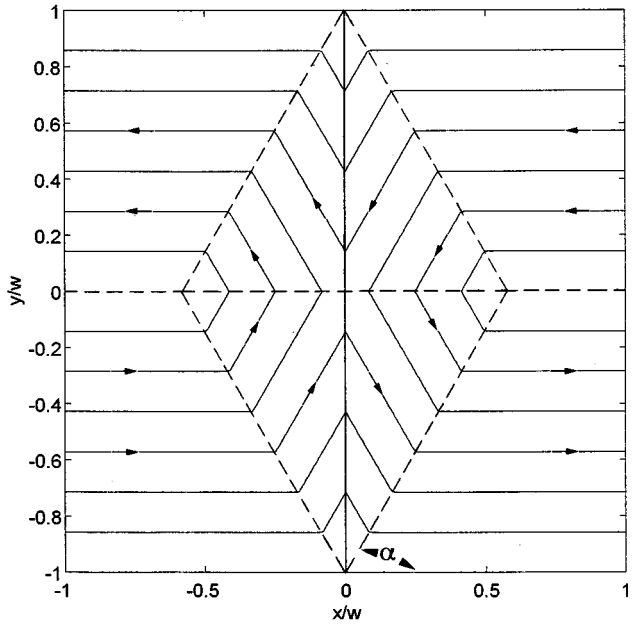

FIG. 10. Current distribution around the grain boundary in the Bean model. The dashed lines show the rhombus produced by the discontinuity lines (d lines) at which the current changes direction.

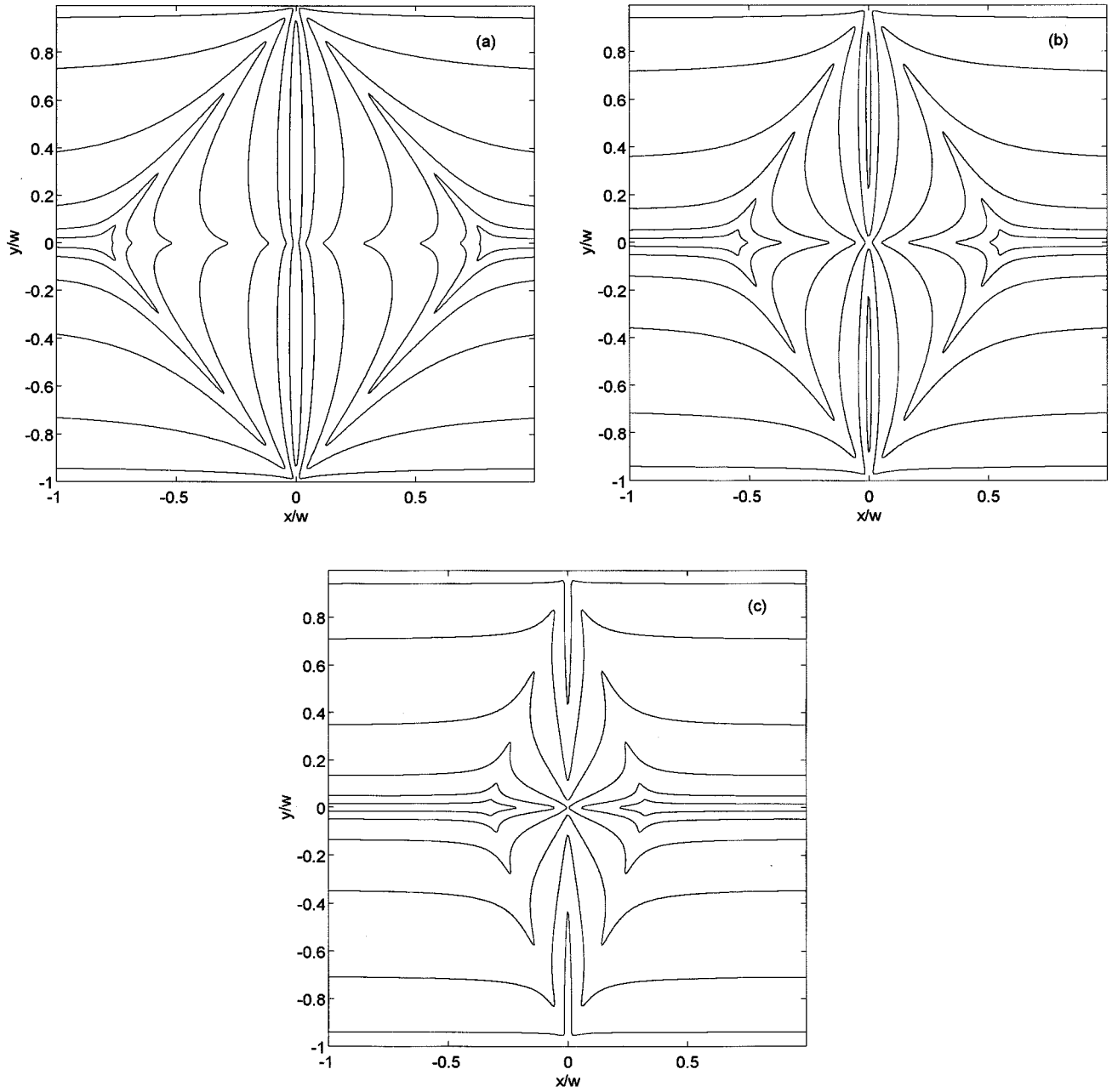

FIG. 11. Contour maps of $B_z(x,y)$ at $z=0.01w$ calculated from Eq. (A1) for $\delta=J_b/J_c=0.2$ (a), 0.5 (b), and 0.8 (c).

the evolution of $B_z(x,y)$ upon changing the grain boundary transmission parameter, $\delta=J_b/J_c$.

Shown in Fig. 11 are contours of $B_z(x,y)$ calculated from Eqs. (2) and (A1) for $z=0.01w$. Here the nonzero z qualitatively accounts for the fact that the observed MO image corresponds to a distance about 3–7 μm away from the sample surface because of the finite thickness of the indicator film, surface irregularities, etc. The contour maps of $B_z(x,y)$ exhibit characteristic cusps on the d lines and on the strip axis, where the tangential component $\mathbf{J}_t(\mathbf{r})$ becomes discontinuous (see Fig. 10). Such cusps are specific to the two-dimensional (2D) current distribution $\mathbf{j}(\mathbf{r},z)=\mathbf{J}(\mathbf{r})\delta(z)$ and appear along any lines of discontinuous $\mathbf{J}_t$. Here the normal component $B_z(x,y)$ has a logarithmic singularity at $z=0$ which turns into a finite peak $B_z(x,y)\sim B_0\ \ln(w/z)$ at the distance z from the surface (a similar effect occurs at $z=0$ if the finite film thickness is taken into account). This results in cusps in $B_z(x,y)$ in the center of a rectangular isotropic strip, for which $J_t(y)=J_c\ \mathrm{sgn}(y)$ at the edges, where $J_t(y)$ abruptly drops from J_c to 0,[56,57] and along the rhombus formed by the contour of the d lines, where J_t changes from $J_c/\sqrt{2}$ to $-J_c/\sqrt{2}$.[49,50] As seen from Fig. 10, the grain boundary should give rise to an additional discontinuity of $\mathbf{J}_t(x,y)$ on the segment $y=0$ inside the d rhombus. This results in a corresponding cusp in $B_z(x,y)$ at $y=0$, which is thus a direct manifestation of a finite J_b across the boundary. This interpretation is in good agreement with the MO images in Figs. 3–6, which do show that the cusp in $B_z(x,y)$ is most pronounced for the 5° bicrystals, for which $J_b\approx(0.5-0.8)J_c$ (see Fig. 1), while for higher-angle grain boundaries with

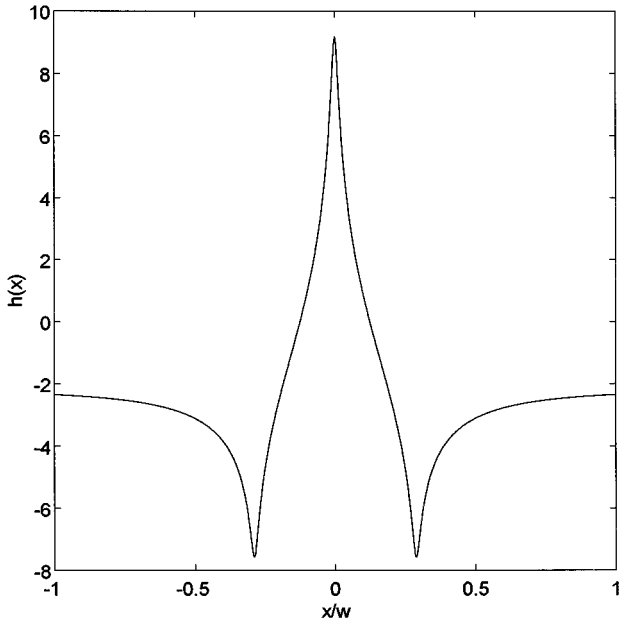

FIG. 12. Flux profile across the boundary calculated from Eq. (A1) for $y=w/2$, $\delta=J_b/J_c=0.5$, and $z=0.01w$.

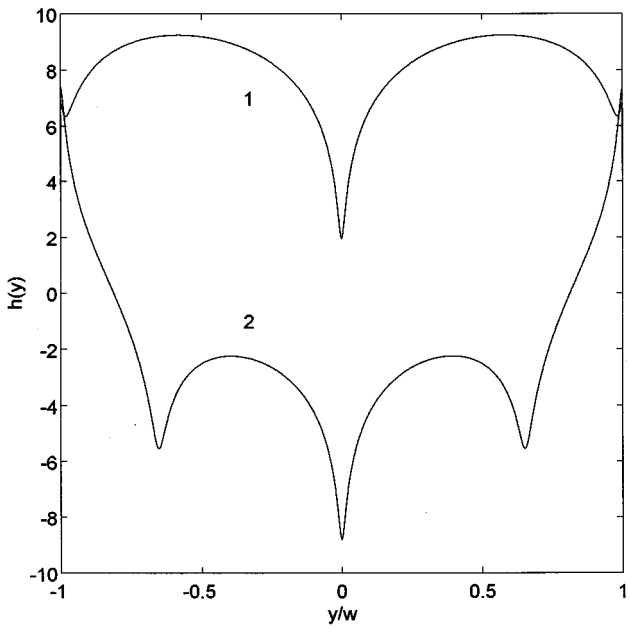

FIG. 13. Flux profiles in the directions parallel to the boundary calculated from Eq. (A1) for $\delta=J_b/J_c=0.5$, $z=0.01w$, and $x=0(1)$, and $x=0.2w(2)$.

$J_b \ll J_c$, the cusp becomes practically invisible, since the boundary almost completely decouples the two parts of the bicrystal.

The above qualitative features of $B_z(x,y)$ also clearly manifest themselves in the flux profiles in the directions parallel and perpendicular to the grain boundary. For instance, Fig. 12 shows the flux profile perpendicular to the boundary calculated from Eq. (A1) for $y=w/2$ and $J_b=J_c/2$. Here the maximum at $x=0$ and the two symmetric minima at $x\approx \pm 0.3w$ result from the discontinuity of J_t at the grain boundary and the d lines, respectively. The calculated $B_z(x,y)$ in Fig. 12 is in good qualitative agreement with the observed flux profile 1 in Fig. 7, although the experimental peaks in $B_z(x,y)$ are smeared out by the effect of Meissner currents due to incomplete flux penetration and the fact that $B_z(x,y)$ was measured at a distance $z\approx 3-7$ μm away from the sample surface. The influence of the Meissner currents also manifests itself in a considerable change of the shape of internal flux profiles 2 and 3, as compared to the profile 1, which corresponds to peripheral regions which are in the critical state.

The calculated flux profiles $B_z(x,y)$ for two different traces parallel to the boundary are shown in Fig. 13. $B_z(x,y)$ experiences sharp dips in the vicinity of the d lines and sharp rises at the film edges. This gives rise to the characteristic nonmonotonic shapes of $B_z(x,y)$ which are also in good qualitative agreement with the measured flux profiles $1'$ and $2'$ in Fig. 8 and are also markedly different from the Bean flux profiles for a slab in a parallel field. The differences are due to the large demagnetizing factor of the perpendicular field orientation, which also results in multiple sign changes of $B_z(x,y)$ and $B_z(x,y)$ in Figs. 12 and 13. The sign reversal of $B_z(x,y)$ can also give rise to alternating regions of positive and negative vortices.[43,64] This is especially pronounced at $H_a=0$ when such a distribution of remanent magnetization is not offset by a strong applied field. Similar nonmonotonic flux profiles along twin boundaries were reported in Ref. 36.

V. TEMPERATURE DEPENDENCIES OF J_b AND J_c

The MO imaging of grain boundaries described in the previous sections permits independent extraction of both J_c and $J_b(\theta)$ for different T. The intragranular critical current density J_c can be obtained both by transport measurements, as described in Sec. III and by measuring the MO flux profiles or the width of the vortex free region[59,60] and then employing the Bean model. In this paper we measure the width of the dark vortex-free region $2b(T,B_a)$ in Figs. 3–5 for different T and then calculate J_c from Eq. (3). Then by measuring the angle $\alpha(T,B_a)$ (see Fig. 9) and using Eq. (1), we extract the ratio J_c/J_b, from which the intergranular critical current density $J_b(T)$ is obtained.

Making use of the data shown in Fig. 9 for the 5° bicrystal and similar but not shown here data for the 7° bicrystal, we plot the ratio $\delta(T)=J_b/J_c$ as a function of T (Fig. 14). For both $\theta=5°$ and $\theta=7°$, the value $\delta(T)$ increases approximately by a factor of 2 as T is increased from 7 to 70 K. Both bicrystals have similar dependencies of $\delta(T)$, although the 7° bicrystal has smaller absolute values of δ ($\sim$0.2 versus $\sim$0.7 for the 5° bicrystal). These results are consistent with the magnetic field transport measurements performed on bicrystal films with the same misorientation angle.[40]

The results of our measurements of $b(B_a)$ for 5° and 7° bicrystals are given in the insets in Figs. 15 and 16, respectively, which show a good fit of Eq. (3) with experiment. This agreement justifies the extraction of the intragrain $J_c(T)$ by inverting Eq. (3): $J_c(T)=\pi B_a/d\mu_0 \cosh^{-1}[w/b(B_a)]$ under the assumption that there is no field dependence of J_c in the low field range $B<100$ mT characteristic of our MO measurements. The temperature dependencies $J_c(T)$ for 5°

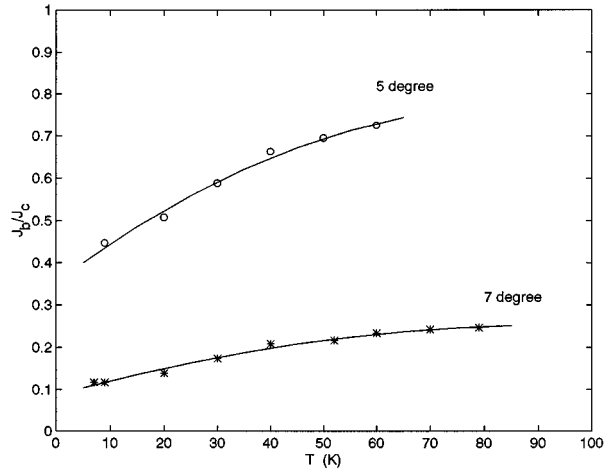

FIG. 14. Temperature dependencies of the ratio $\delta=J_b/J_c$ calculated from Eq. (1) using the data shown in Fig. 9 for the 5° boundary and likewise for the 7° boundary.

and 7° bicrystals obtained are shown in Figs. 15 and 16, respectively. These J_c data, when combined with the measured ratio J_b/J_c in Fig. 14, allow us to extract the intergranular $J_b(T)$ without any contribution from the series intragranular regions, as inevitably occurs in transport measurements. The temperature-dependent $J_b(T)$ data for $\theta=5°$ and 7° are also shown in Figs. 15 and 16. $J_b(T)$ for both $\theta=5°$ and 7° is less temperature dependent then $J_c(T)$, which results in the somewhat unexpected increase of $\delta(T)=J_b/J_c$ with T in Fig. 14. Figure 17 shows the temperature dependence of the ratio $J_b(7°,T)/J_b(5°,T)$. Therefore, the noticeable differences in J_b for 5° and 7° bicrystals at low temperatures become less pronounced at higher T.

A qualitative interpretation of this behavior of $J_b(\theta,T)$ can be given based on the microstructure of low-angle grain boundaries which are not continuous interfaces but rather a

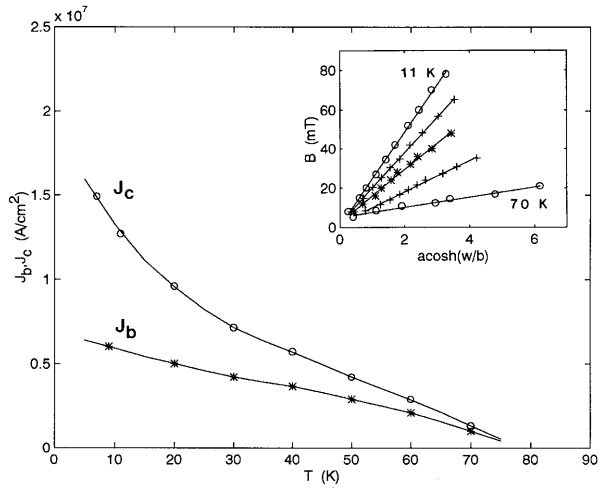

FIG. 15. Temperature dependence of the intragrain J_c (upper curve) for the 5° bicrystal calculated from MO images by using Eq. (3). The lower curve shows the temperature dependence of J_b for the 5° grain boundary extracted from the data in Fig. 14 and $J_c(T)$. The inset shows the linear fit of the observed width of Meissner region $2b(B_a)$ to Eq. (3) for $T=11$, 20, 30, 50, and 70 K.

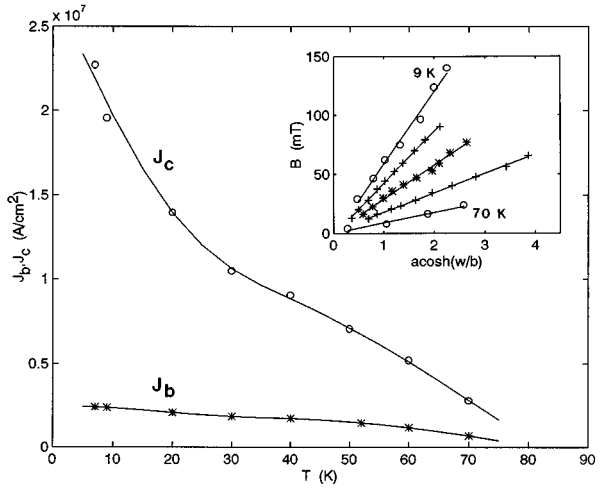

FIG. 16. Temperature dependence of the intragrain J_c (upper curve) for the 7° bicrystal calculated from MO images by using Eq. (3). The lower curve shows the temperature dependence of J_b for the 7° grain boundary extracted from the data in Fig. 14 and $J_c(T)$. The inset shows the linear fit of the observed width of Meissner region $2b(B_a)$ to Eq. (3) for $T=9$, 20, 40, 60, and 70 K

chain of edge dislocations separated by regions of comparatively undisturbed lattice.[3,9,40] The critical misorientation angle θ_c, where the cores start to overlap is between 10° and 15°.[9] The dislocation cores are believed to suppress T_c locally such that the normal regions of and around the core decrease J_b by reducing the cross section available for supercurrents flowing through the grain boundary.[9] At the same time, the chain of dislocation cores could provide additional pinning of intergrain vortices, thus increasing J_b as θ is increased. This extra flux pinning may become more significant at higher temperatures for which thermal fluctuations reduce the 3D intragrain pinning more strongly than they do the 1D intergrain dislocation core pinning.[65] As a result, the

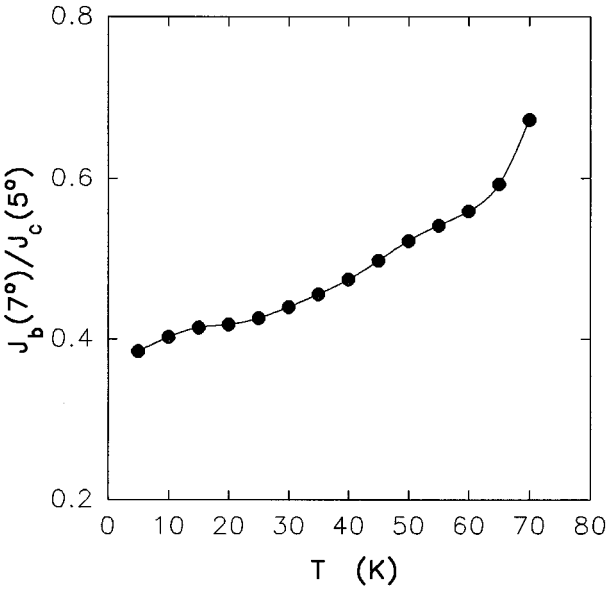

FIG. 17. Temperature dependence of the ratio $J_b(7°,T)/J_b(5°,T)$ obtained from the data of Figs. 15 and 16.

reduction of the current-carrying cross section by dislocation cores can significantly reduce $J_b(\theta,T)$ at lower T, while the difference between J_b and J_c becomes less pronounced at higher T due to the effect of thermal fluctuations. These opposing trends can account for the observed increase of the ratios J_b/J_c and $J_b(7°,T)/J_b(5°,T)$ with increasing temperature, which are quite different from those exhibited by high-angle grain boundaries which behave as continuous, long Josephson contacts.

VI. CONCLUSION

We have shown that the MO imaging technique can be usefully applied to the study of magnetic flux and current distributions in $YBa_2Cu_3O_{7-\delta}$ bicrystals. By making a quantitative analysis of $B_z(x,y)$ for different misorientation angles θ, we have shown that a characteristic cusp in $B_z(x,y)$ appears as the grain boundary begins exerting a significant barrier to magnetization currents. We were able to model this cusp and other characteristic features of the observed flux distributions $B_z(x,y)$ using a thin-film Bean model which also enabled us to extract both J_b and J_c independently from the experimental data. A particular advantage of the MO technique for these studies is that the intergrain critical current density J_b can be derived without series contributions from the grains, as is inevitably the case in transport measurements. It is shown that the intergrain $J_b(\theta,T)$ exhibits weaker temperature dependencies than the intragrain J_c, which we attribute to additional flux pinning at the grain boundaries provided by the grain boundary dislocations.

ACKNOWLEDGMENTS

We are grateful to E. H. Brandt, J. R. Clem, V. I. Nikitenko, and V. K. Vlasko-Vlasov for useful discussions. This work was supported by the NSF MRG Program (DRM-9214707).

APPENDIX

To calculate $B_z(x,y)$ it is convenient to write Eq. (2) as follows:

$$h(x,y)=h_1(x,y)+h_2(x,y)+h_3(x,y), \tag{A1}$$

where $h(\mathbf{r})=4\pi B(\mathbf{r})/dJ_c\mu_0$ is a dimensionless magnetic field, and all coordinates are measured in units of w. Here

$$h_1(y)=\ln\frac{(1+y^2+z^2)^2-4y^2}{(y^2+z^2)^2} \tag{A2}$$

is the field distribution around an infinite strip in the absence of the grain boundary at $B\gg B_0$. The values h_2 and h_3 are given by

$$h_2(x,y)=(\delta-1)\int_{-c}^{c}dx'\int_{-1+t|x'|}^{1-t|x'|}\times dy'\frac{(y-y')\mathrm{sgn}(y')}{[(x-x')^2+(y-y')^2+z^2]^{3/2}}, \tag{A3}$$

$$h_3(x,y)=-\sqrt{1-\delta^2}\int_{-1}^{1}dy'\int_{-(1-|y'|)t}^{(1-|y'|)t}\times dx'\frac{(x-x')\mathrm{sgn}(x')}{[(x-x')^2+(y-y')^2+z^2]^{3/2}}, \tag{A4}$$

where $t=\tan\alpha$ and $c=\cot\alpha$. Here h_2 and h_3 are the magnetic fields produced by the x and y components of $\mathbf{J}(\mathbf{r})$ inside the d rhombus shown in Fig. 8 with $J_x=J_b-J_c$ and $J_y=(J_c^2-J_b^2)^{1/2}$, respectively. A straightforward calculation of the integrals in Eqs. (A3) and (A4) yields

$$h_2=(\delta-1)\left\{2\ln\frac{f_1+c-x}{f_2-c-x}-\frac{1}{\beta}\ln\frac{[\beta f_1+c-x]^2-t^2y^2}{[\beta g_1-t(1-y)^2]^2-x^2}-\frac{1}{\beta}\ln\frac{[\beta f_2+c+x]^2-t^2y^2}{[\beta g_2-t(1+y)^2]^2-x^2}\right\}, \tag{A5}$$

$$h_3=\sqrt{1-\delta^2}\left\{\frac{t}{\beta}\ln\frac{[\beta g_1+t(1-y)]^2-x^2}{[\beta f_1-c+x]^2-t^2y^2}+\frac{t}{\beta}\ln\frac{[\beta g_2+t(1+y)]^2-x^2}{[\beta f_2-c-x]^2-t^2y^2}-2\ln\frac{g_1+1-y}{g_2-1-y}\right\}, \tag{A6}$$

$$f_{1,2}=\sqrt{y^2+z^2+(x\mp 1/t)^2},\quad g_{1,2}=\sqrt{x^2+z^2+(1\mp y)^2}, \tag{A7}$$

$$t=\sqrt{\frac{1+\delta}{1-\delta}},\quad \beta=\sqrt{\frac{2}{1-\delta}}. \tag{A8}$$

In this calculation we neglect flux creep which can give rise to singnificant inhomogeneities of electric field along *GB*.[66]

*Also at the Institute of Solid State Physics, Russian Academy of Sciences, Chernogolovka, Moscow District, 142432 Russia.
†Also at the Department of Electrical and Computer Engineering, University of Wisconsin, Madison, Wisconsin 53706.
‡Also at the Department of Material Science and Engineering, University of Wisconsin, Madison, Wisconsin 53706.

[1] G. Deutscher and K. A. Müller, Phys. Rev. Lett. **59**, 1745 (1987).
[2] P. Chaudhari, J. Mannhart, D. Dimos, C. C. Tsuei, J. Chi, M. Oprysko, and M. Scheuermann, Phys. Rev. Lett. **60**, 1653 (1988); D. Dimos, P. Chaudhari, J. Mannhart, and F. K. LeGoues, *ibid.* **61**, 219 (1988); J. Mannhart, P. Chaudhari, D. Dimos, C. C. Tsuei, and T. R. McGuire, *ibid.* **61**, 2476 (1988).
[3] D. Dimos, P. Chaudhari, and J. Mannhart, Phys. Rev. B **41**, 4038 (1990).
[4] Z. G. Ivanov, P. A. Nilsson, D. Winkler, J. A. Alarco, T. Claeson, E. A. Stepantsov, and A. Ya. Tzalenchuk, Appl. Phys. Lett. **59**, 3030 (1991).
[5] D. K. Lathrop, B. H. Moeckly, S. E. Russek, and R. A. Buhrman, Appl. Phys. Lett. **58**, 1095 (1991).
[6] M. Strikovsky, G. Linker, S. Gaponov, I. Mazo, and O. Mayer, Phys. Rev. B **45**, 12 522 (1992).
[7] R. Gross and B. Mayer, Physica C **180**, 235 (1991).
[8] R. Gross, in *Interfaces in High-T_c Superconducting Systems*, edited by S. L. Shinde and D. A. Rudman (Springer-Verlag, New York, 1993), p. 176.
[9] M. F. Chisholm and S. J. Pennycook, Nature **351**, 47 (1991).
[10] A. H. Cardona, H. Suzuki, T. Yamashita, K. H. Young, and L. C. Bourne, Appl. Phys. Lett. **62**, 411 (1993).

[11] B. Mayer, L. Alff, T. Trauble, and R. Gross, Appl. Phys. Lett. **63**, 996 (1993).
[12] M. Kawasaki, E. Sarnelli, P. Chaudhari, A. Gupta, A. Kussmaul, J. Lacey, and W. Lee, Appl. Phys. Lett. **62**, 417 (1993).
[13] E. Sarnelli, P. Chaudhari, W. Y. Lee, and E. Esposito, Appl. Phys. Lett. **65**, 362 (1994).
[14] T. Nabatame, S. Koike, O. B. Hyun, and I. Hirabayashi, Appl. Phys. Lett. **65**, 776 (1994).
[15] A. Marx, U. Fath, W. Ludwig, R. Gross, and T. Amrein, Phys. Rev. B **51**, 6735 (1995).
[16] T. Amrein, L. Schultz, B. Kabius, and K. Urban, Phys. Rev. B **51**, 6792 (1995).
[17] S. E. Babcock, X. Y. Cai, D. L. Kaiser, and D. C. Larbalestier, Nature **347**, 167 (1990).
[18] D. C. Larbalestier, S. E. Babcock, X. Y. Cai, M. B. Field, Y. Gao, N. F. Heinig, D. L. Kaiser, K. Merkle, L. K. Williams, and N. Zhang, Physica C **185–189**, 315 (1991).
[19] C. B. Eom, A. F. Marshall, Y. Suzuki, B. Boyer, R. F. W. Pease, and T. H. Geballe, Nature **353**, 544 (1991).
[20] G. Gartz, T. Schield, N. Bouadma, F. R. Ladan, P. Gabelotaund, and C. Gonzalez, Physica C **235–240**, 3061 (1994).
[21] A. Marshall, J. Met. **47**(3), 43 (1995).
[22] A. Forkl, T. Dragon, and H. Kronmüller, J. Appl. Phys. **67**, 3047 (1990); Th. Schuster, M. R. Koblischka, H. Kuhn, and H. Kronmüller, Appl. Phys. Lett. **62**, 168 (1993); M. R. Koblischka, Th. Schuster, and H. Kronmüller, Physica C **219**, 205 (1994); R. Hedderich, Th. Schuster, H. Kuhn, J. Geerk, G. Linker, and M. Murakami, Appl. Phys. Lett. **66**, 3215 (1995).
[23] N. Nakamura, G. D. Gu, K. Takamuku, M. Murakami, and N. Koshizuka, Appl. Phys. Lett. **61**, 3044 (1992); T. Egi, J. G. Wen, H. Kubota, J. Ricketts, and N. Koshizuka, *ibid.* **66**, 3680 (1995).
[24] Th. Schuster, M. R. Koblischka, H. Kuhn, and H. Kronmüller, Appl. Phys. Lett. **62**, 768 (1993).
[25] V. K. Vlasko-Vlasov, V. N. Goncharov, V. I. Nikitenko, A. A. Polyanskii, I. F. Voloshin, L. M. Fisher, N. M. Aleshina, and O. A. Poluschenko, Physica C **222**, 367 (1994).
[26] M. Turchinskaya, D. L. Kaiser, F. W. Gayle, A. J. Shapiro, A. Roytburd, L. A. Dorosinskii, V. I. Nikitenko, A. A. Polyanskii, and V. K. Vlasko-Vlasov, Physica C **221**, 62 (1994).
[27] Y. Yokoyama, T. Kubo, Y. Nakagawa, M. Umeda, Y. Suzuki, and S. Yoshida, Physica C **219**, 327 (1994).
[28] D. C. Larbalestier X. Y. Cai, H. Edelman, M. B. Field, Y. Feng, J. Parrell, A. Pashitski, and A. Polyanskii, J. Met. **46**(12), 20 (1994).
[29] M. Field, A. Pashitski, A. Polyanskii, and D. C. Larbalestier, IEEE Trans. Appl. Supercond. **5**, 1631 (1995).
[30] C. A. Duran, P. L. Gammel, R. Wolfe, V. J. Fratello, D. J. Bishop, J. P. Rice, and D. M. Ginsberg, Nature **357**, 474 (1992).
[31] V. K. Vlasko-Vlasov, M. V. Indenbom, and A. A. Polyanskii, in *The Real Structure of High-T_c Superconductors*, edited by V. Sh. Shekhtman, Springer Series in Materials Science Vol. 23 (Springer-Verlag, Berlin, 1993), p. 111.
[32] M. Turchinskaya, D. L. Kaiser, F. W. Gayle, A. J. Shapiro, A. Roytburd, V. K. Vlasko-Vlasov, A. A. Polyanskii, and V. I. Nikitenko, Physica C **216**, 205 (1993).
[33] L. A. Dorosinskii, M. V. Indenbom, V. I. Nikitenko, A. A. Polyanskii, R. L. Prozorov, and V. K. Vlasko-Vlasov, Physica C **206**, 360 (1993).
[34] L. A. Dorosinskii, V. I. Nikitenko, A. A. Polyanskii, and V. K. Vlasko-Vlasov, Physica C **219**, 81 (1994).
[35] V. K. Vlasko-Vlasov, L. A. Dorosinskii, A. A. Polyanskii, V. I. Nikitenko, U. Welp, B. W. Veal, and G. W. Crabtree, Phys. Rev. Lett. **72**, 3246 (1994).
[36] U. Welp, T. Gardiner, D. Gunter, J. Fendrich, G. W. Crabtree, V. K. Vlasko-Vlasov, and V. I. Nikitenko, Physica C **235–240**, 241 (1994).
[37] L. A. Dorosinskii, M. V. Indenbom, V. I. Nikitenko, A. A. Polyanskii, and V. K. Vlasko-Vlasov, Physica C **235–240**, 2727 (1994).
[38] J. Mannhart, R. Gross, K. Hipler, R. P. Huebener, C. C. Tsuei, D. Dimos, and P. Chaudhari, Science **245**, 839 (1989); J. Mannhart, R. P. Huebener, F. Kober, D. Koelle, P. Chaudhari, D. Dimos, R. Gross, A. Gupta, G. Koren, and C. C. Tsuei, Physica A **168**, 345 (1990); R. Gerdermann, K.-D. Husemann, R. Gross, L. Alff, A. Beck, B. Elia, W. Reuter, and M. Siegel, J. Appl. Phys. **76**, 8005 (1994).
[39] X. D. Wu, S. R. Foltyn, P. N. Arendt, W. R. Blumenthal, I. H. Campbell, J. D. Cotton, J. Y. Coulter, W. L. Hults, M. P. Maley, H. F. Safar, and J. L. Smith, Appl. Phys. Lett. **67**, 2397 (1995).
[40] N. F. Heinig, R. D. Redwing, I.-F. Tsu, A. Gurevich, J. E. Nordman, S. E. Babcock, and D. C. Larbaletier (unpublished).
[41] Y. Iijima, N. Tanabe, O. Kohno, and Y. Ikeno, Appl. Phys. Lett. **60**, 769 (1992).
[42] R. P. Reade, P. Berdahl, R. E. Russo, and S. M. Garrison, Appl. Phys. Lett. **61**, 2231 (1992).
[43] L A. Dorosinskii, M. V. Indenbom, V. I. Nikitenko, Yu. A. Ossip'yan, A. A. Polyanskii, and V. K. Vlasko-Vlasov, Physica C **203**, 149 (1992).
[44] M. R. Koblischka and R. J. Wijngaarden, Supercond. Sci. Technol. **8**, 199 (1995).
[45] A. E. Pashitski, A. Polyanskii, A. Gurevich, J. A. Parrell, and D. C. Larbalestier, Physica C **246**, 133 (1995).
[46] A. E. Pashitski, A. Polyanskii, A. Gurevich, J. A. Parrell, and D. C. Larbalestier, Appl. Phys. Lett. **67**, 2720 (1995).
[47] R. P. Huebener, V. A. Rowe, and R. T. Kampwirth, J. Appl. Phys. **41**, 2963 (1970).
[48] P. Brüll, D. Kirschässner, and P. Leiderer, Physica C **182**, 339 (1991).
[49] V. K. Vlasko-Vlasov, M. V. Indenbom, V. I. Nikitenko, A. A. Polyanskii, R. L. Prozorov, I. V. Grekhov, L. A. Delimova, I. A. Liniichuck, A. V. Antonov, and M. Yu. Gusev, Superconductivity **5**, 1582 (1992).
[50] Th. Schuster, M. V. Indenbom, M. R. Koblischka, H. Kuhn, and H. Kronmüller, Phys. Rev. B **49**, 3443 (1994).
[51] E. H. Brandt, Phys. Rev. Lett. **74**, 3025 (1995).
[52] W. T. Norris, J. Phys. D **3**, 489 (1970).
[53] D. J. Frankel, J. Appl. Phys. **50**, 5402 (1979).
[54] M. Däumling and D. C. Larbalestier, Phys. Rev. B **40**, 9350 (1989).
[55] H. Theuss, A. Forkl, and H. Kronmüller, Physica C **190**, 345 (1992).
[56] E. H. Brandt, M. Indenbom, and A. Forkl, Europhys. Lett. **22**, 735 (1993); E. H. Brandt and M. Indenbom, Phys. Rev. B **48**, 12 893 (1993).
[57] E. Zeldov, J. R. Clem, M. McElfresh, and M. Darwin, Phys. Rev. B **49**, 9802 (1994).
[58] E. Zeldov, A. I. Larkin, V. B. Geshkenbein, M. Konczykowski, D. Majer, B. Khaykovich, V. M. Vinokur, and H. Shtrikman, Phys. Rev. Lett. **73**, 1428 (1994).
[59] Th. Schuster, H. Kuhn, E. H. Brandt, M. Indenbom, M. R. Koblischka, and M. Konczykowski, Phys. Rev. B **50**, 16 684 (1994).

[60] R. Knorpp, A. Forkl, H.-U. Habermeier, and H. Kronmüller, Physica **230**, 128 (1994).
[61] C. P. Bean, Rev. Mod. Phys. **36**, 31 (1964).
[62] A. M. Campbell and J. E. Evetts, *Critical Currents in Superconductors* (Taylor & Frances, London, 1972).
[63] E. M. Gyorgy, R. B. van Dover, K. A. Jackson, L. F. Schneemeyer, and J. V. Waszczak, Appl. Phys. Lett. **55**, 283 (1989).
[64] Th. Schuster, M. R. Koblischka, B. Ludescher, and H. Kronmüller, J. Appl. Phys. **72**, 1478 (1992); Th. Schuster, M. R. Koblischka, H. Kuhn, B. Ludescher, M. Leghissa, M. Lippert, and H. Kronmüller, Physica C **196**, 373 (1992).
[65] G. Blatter, M. V. Feigelman, V. B. Geshkenbein, A. I. Larkin, and V. M. Vinokur, Rev. Mod. Phys. **66**, 1125 (1994).
[66] Th. Schuster, H. Kuhn, E. H. Brandt, M. V. Indenbom, M. Kläser, G. Müller-Vogt, H.-U. Habermeier, K. Kronmüller, and A. Forkl, Phys. Rev. B **52**, 10 375 (1995).